Tropopause-level thin cirrus coverage revealed by ICESat/Geoscience Laser Altimeter System

A. E. Dessler,[1] S. P. Palm,[2] W. D. Hart,[2] and J. D. Spinhirne[3]

Received 12 August 2005; revised 31 October 2005; accepted 20 December 2005; published 26 April 2006.

[1] We analyze the distribution of thin (optical depth < 0.40) cirrus in the tropics at potential temperatures of 360, 370, 377.5, and 400 K, which are levels that bracket the tropical tropopause. The observations were obtained between 29 September and 17 November 2003 by the Geoscience Laser Altimeter System (GLAS), carried on board the Ice, Cloud, and land Elevation Satellite (ICESat). The GLAS data show that these thin, near-tropopause cirrus (TNTC) occur over broad regions of the latitude range 20°S to 30°N, with distinct maxima collocated with regions of intense convection, and that TNTC occurrence frequency decreases strongly with increasing altitude. At 377.5 K, approximately the level of the tropical tropopause, TNTC frequency over convection is two to six times larger than in the so-called "cold pool," the climatological temperature minimum located over the equatorial western Pacific where it has been suggested that dehydration of air entering the stratosphere is occurring. Comparisons between assimilated temperatures, outgoing longwave radiation (a proxy for deep convection), and TNTC frequency show that TNTC can be found where assimilated temperatures are low and deep convection is occurring. We find that assimilated temperatures, by themselves, are incomplete predictors of TNTC locations.

Citation: Dessler, A. E., S. P. Palm, W. D. Hart, and J. D. Spinhirne (2006), Tropopause-level thin cirrus coverage revealed by ICESat/Geoscience Laser Altimeter System, *J. Geophys. Res.*, *111*, D08203, doi:10.1029/2005JD006586.

1. Introduction

[2] In recent years, it has become clear that the troposphere and stratosphere are separated by a transition layer several kilometers thick [e.g., *Atticks and Robinson*, 1983; *Highwood and Hoskins*, 1998; *Folkins et al.*, 1999]. While various definitions exist for this layer, often referred to as the tropical tropopause layer (TTL), one oft-cited definition puts the bottom boundary at the level of zero net radiative heating [*Sherwood and Dessler*, 2000, 2001], which occurs between 14.5- to 16-km altitude or 355- to 365-K potential temperature [*Folkins et al.*, 1999; *Gettelman et al.*, 2004]. Air below the zero net radiative heating line is radiatively cooling, sinking back to the surface as part of the tropical overturning Hadley or Walker circulations. Air above this level experiences radiative heating and rises toward the stratosphere. The upper limit of the TTL is the level where overshooting convection tails off, around 18 km [e.g., *Alcala and Dessler*, 2002]. The tropopause lies within the TTL; various definitions of the tropopause exist, but they all put its location somewhere around 375- to 380-K potential temperature, about 1–2 km or 15- to 25-K potential temperature above the base of the TTL.

[3] Thin (optical depth $\ll$1) cirrus within a kilometer or so of the tropopause have recently garnered much attention by the scientific community. They are potentially radiatively important [e.g., *McFarquhar et al.*, 2000; *Hartmann et al.*, 2001; *Jensen et al.*, 1996] and potentially play a role in dehydration of air entering the stratosphere [e.g., *Holton and Gettelman*, 2001; *Gettelman et al.*, 2002; *Jensen and Pfister*, 2004; *Luo et al.*, 2003]. While there are several analyses of observations of these clouds [*Wang et al.*, 1996; *Winker and Trepte*, 1998; *McFarquhar et al.*, 2000; *Mergenthaler et al.*, 1999; *Nee et al.*, 1998; *Sassen and Cho*, 1992; *Dessler and Yang*, 2003; *Peter et al.*, 2003], much about their distribution and formation mechanisms remain uncertain, owing primarily to the difficulty of observing them. In this paper, we present an analysis of these clouds using a new, highly accurate satellite-borne lidar data set, and discuss the implications of the analysis for our understanding of these clouds' formation mechanisms as well as our understanding of the dehydration of air entering the stratosphere.

2. ICESat/GLAS Measurements

[4] The Geoscience Laser Altimeter System (GLAS), carried onboard the Ice, Cloud, and land Elevation Satellite (ICESat), is a diode-pumped Q-switched Nd:YAG laser operating in the near infrared (1064 nm) and visible (532 nm). Measurements of attenuated backscatter from the instrument are processed by the science team to produce high-quality measurements of cloud properties over most of

[1]Department of Atmospheric Sciences, Texas A&M University, College Station, Texas, USA.
[2]Science Systems and Applications Inc., Lanham, Maryland, USA.
[3]NASA Goddard Space Flight Center, Greenbelt, Maryland, USA.

0148-0227/06/2005JD006586

the globe [*Spinhirne et al.*, 2005; *Zwally et al.*, 2002]. During the period analyzed in this paper, 29 September to 17 November 2003 (the so-called "Laser 2a" period), the measurements in the tropics were obtained around 8 am and 8 pm local solar time. Morning observations occurred during daylight, with solar zenith angles ranging from 53° to 85°. Evening observations occurred after sunset, with solar zenith angles ranging from 95° to 128°.

[5] While the GLAS has two wavelengths, the data analyzed in this paper are based exclusively on the 532-nm data. The 532-nm channel of GLAS employs four Single Photon Counting Modules (SPCMs), which have high sensitivity and low noise characteristics that are optimal for thin cloud detection. GLAS can measure optical depth down to about 0.002 at night and 0.02 during the day, with an uncertainty of 20% to 50% [*Hlavka et al.*, 2005; *Palm et al.*, 2002].

[6] The SPCMs are sampled at 1.953 MHz, which translates to a vertical resolution of 76.8 m. In this paper, we use the cloud tops and bottoms identified in the release 19 GLA09 data product [*Hart et al.*, 2005; *Palm et al.*, 2002]. This algorithm averages 4 s (160 laser shots) of calibrated, 532-nm attenuated backscatter to obtain one vertical profile that is then examined for the locations of layers that exceed a threshold based on the magnitude of molecular backscatter and background noise. A cloud layer top is defined as that height where the first of two consecutive GLAS data bins of 76.8 m (from above the cloud moving downward) exceed the threshold; the bottom is that height where the first of two consecutive bins are less than the threshold (from within the cloud moving downward). During the 4-s period, the satellite moves about 28 km, so this distance defines the scale of features we are investigating. For a thorough discussion of the instrument and its atmospheric measurements, see *Spinhirne et al.* [2005] and the ICESat/GLAS special section (*Geophysical Research Letters*, 32(21–22), 2005).

[7] Although the GLA09 algorithm requires two backscatter measurements to exceed a threshold before a cloud edge is detected, the top bin will virtually always contain the top of the cloud. Thus the inherent uncertainty of the cloud height is equal to the SPCM resolution of 76.8 m. In addition, GLAS measurements of cloud altitude are made with respect to the geoid, an equipotential surface of the Earth's gravity field that most closely approximates mean sea level (MSL). Differences between the geoid and MSL can be as much as a few tens of meters. Combining all of the sources of uncertainty produces a total uncertainty in cloud height above MSL of less than 100 m.

[8] To facilitate our analysis of TTL thin cirrus, we will convert GLAS measurements of geometric altitude to potential temperature using assimilated meteorological fields from the United Kingdom Meteorological Office (UKMO) [*Swinbank and O'Neill*, 1994], which are produced on a regular grid once per day. To calculate the potential temperature of each cloud boundary, we assume that geometric height above the geoid, which is measured by GLAS, and geopotential height, which is reported in the meteorological data sets, are equivalent. We then generate a geopotential height-potential temperature relation for the location of the GLAS measurement by interpolation of the UKMO meteorological fields to determine the potential temperature of the cloud edges. This conversion introduces additional uncertainties. The assumption that geometric height equals geopotential height introduces an error of several tens of meters in the upper troposphere, corresponding to an error of a few tenths of a degree K of θ. More significant are errors in the meteorological fields. The UKMO temperature fields tend to be warm-biased around the tropopause by as much as 3 K [*Randel et al.*, 2000], which translates into an the uncertainty in cloud θ in the neighborhood of 5–6 K.

3. Tropopause-Level Thin Cirrus

[9] We classify a thin, near-tropopause cirrus (TNTC) at a given level as any cloud whose top and bottom bracket that level (e.g., 360-K TNTC are those with tops above 360 K and bottoms below 360 K) and whose simultaneously measured optical depth (τ), as reported in the release 19 GLA11 product, is below 0.40. The GLA11 algorithm uses a signal-loss method to estimate the optical depth for the thin clouds analyzed here. See *Palm et al.* [2002] for the details of the algorithm.

[10] This optical depth screen is designed to include thin cirrus but eliminate convective and thick anvil clouds from the analysis. About 62% of clouds with tops above 355 K have τ below 0.40, 30% have τ between 0.40 and $\sim$3, and 8% have τ greater than $\sim$3. We will discuss the sensitivity to this optical depth screen later. Finally, we include all clouds fitting the criteria for TNTC in the analysis, irrespective of whether there are clouds above or below them.

[11] In this paper, we will analyze TNTC occurrence at four potential temperatures: 360, 370, 377.5, and 400 K, corresponding to geometric altitudes of 13.7–15.8, 14.6–16.8, 15.1–17.4, and 16.2–18.5 km (altitude ranges are one standard deviation about the mean, calculated from meteorological data obtained from the Global Positional Satellite (GPS) system [e.g., *Rocken et al.*, 1997; *Randel et al.*, 2003; *Hajj et al.*, 2004]). The 360-K potential temperature surface is around the base of the TTL; the 370-K surface is about halfway between the base of the TTL and the tropopause; the 377.5-K surface is the average height of the cold-point tropical tropopause during the laser-2a period; the 400-K surface is $\sim$1 km above the tropopause.

[12] Figures 1–4 show the horizontal distribution of TNTC frequency (the number of observations that show a TNTC divided by the total number of observations). Virtually all of the plots show, to a greater or lesser extent, maxima in the TNTC distribution in three general locations. Two of these maxima are found over continental regions: equatorial Africa and South America. The locations of these continental maxima are approximately in the same location at all altitudes in the TTL. The third is a large maximum over the western Pacific. At 360 K, the western Pacific maximum is approximately centered over the equator, while at higher potential temperatures it shifts to the north of the equator. In total, 4.6, 1.3, 0.5, and 0.04% of the GLAS morning observations between 20°S and 30°N see a TNTC at 360, 370, 377.5, and 400 K, respectively. In the evening, the TNTC frequencies are 9.5, 5.6, 3.2, and 0.5%.

[13] Had we included all clouds that the GLAS laser can penetrate ($\tau < \sim 3-4$) instead of limiting ourselves to those with $\tau < 0.40$, we would have found daytime frequencies of 6.9, 2.2, 0.9, 0.08% and nighttime frequencies of 13.7, 7.0,

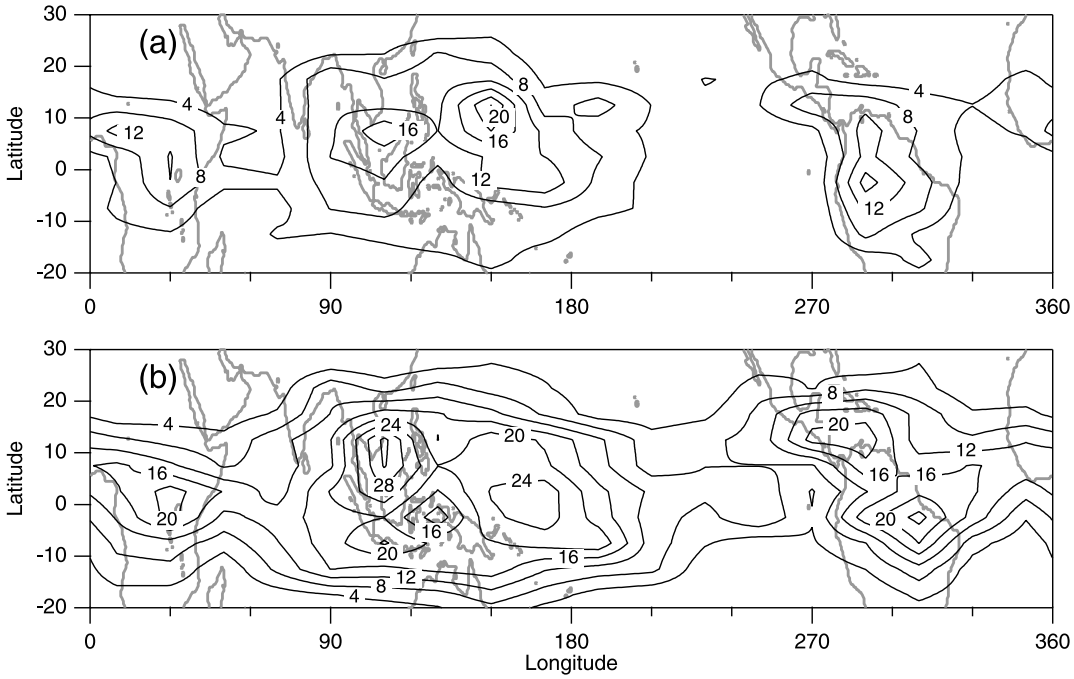

Figure 1. Fraction of GLAS observations (in percent) containing a TNTC at 360-K potential temperature, (a) morning data and (b) evening data. The contour interval is 4%.

3.9, 0.6%. Figures 1–4 would have looked similar, except the TNTC frequency would be increased by a factor of ~1.3.

[14] While distinct maxima are clearly visible, TNTC occurrence is also widespread, with the 3% contour covering one half to three quarters of the area at night between 20°S and 30°N at 360, 370, and 377.5 K. TNTC become less frequent as altitude increases, but we note that 400 K is not the highest level that GLAS observes TNTC. Rather, TNTC occur with decreasing frequency up to about 420 K, with maxima remaining in the same locations.

[15] The location of the maxima in TNTC occurrence is virtually the same in the morning and evening on all three levels, suggesting that there is little diurnal cycle in the

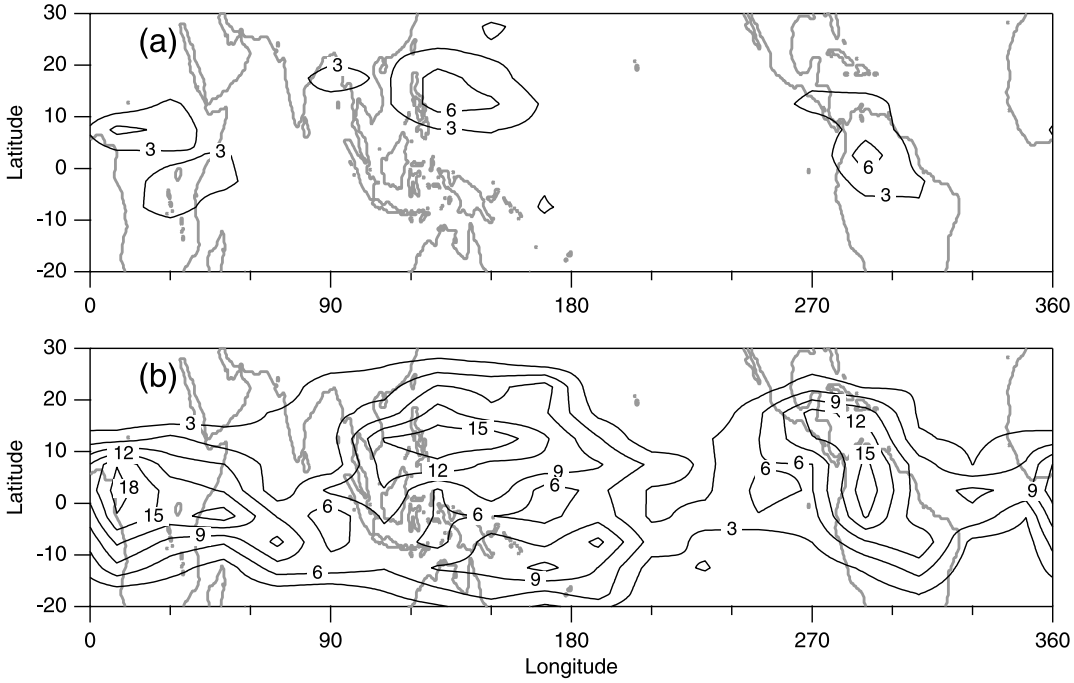

Figure 2. Fraction of GLAS observations (in percent) containing a TNTC at 370-K potential temperature, (a) morning data and (b) evening data. The contour interval is 3%.

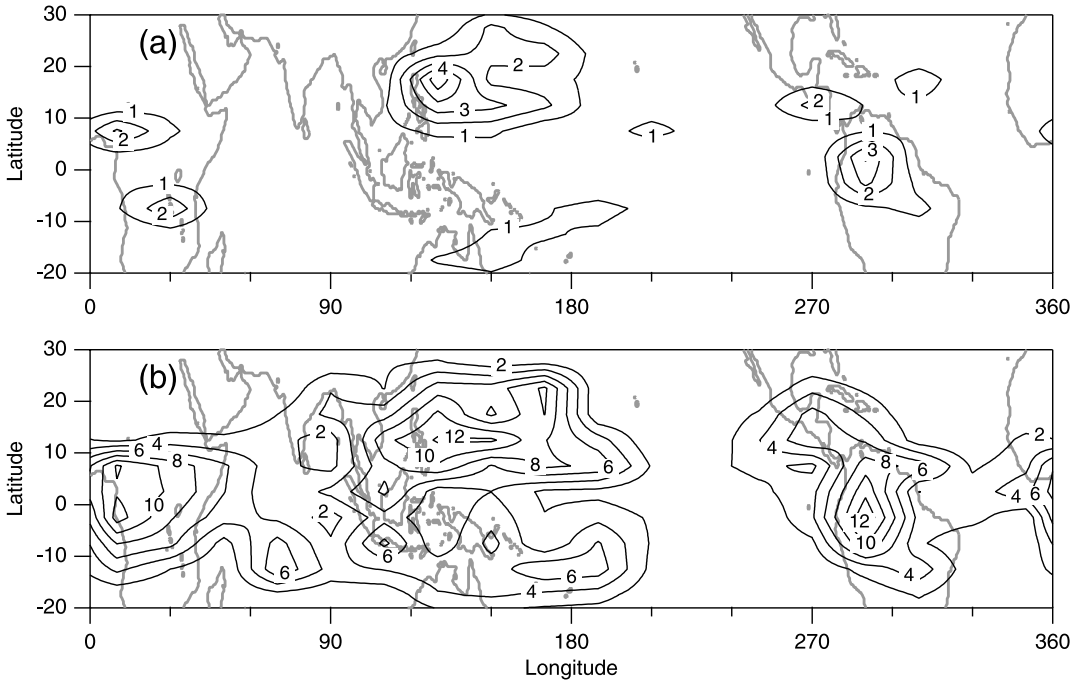

Figure 3. Fraction of GLAS observations (in percent) containing a TNTC at 377.5-K potential temperature, (a) morning data and (b) evening data. The contour interval is 1% for the morning plot and 2% for the evening plot.

location of TNTC. There are fewer observations of TNTC in the morning than in the evening at all four levels. One must be careful about interpreting this diurnal cycle, however, since the greater sensitivity of the GLAS during night (when there is no solar 532-nm radiation to confound the measurement) is making a contribution of unknown magnitude to the diurnal cycle. It may be possible to use the GLAS1064-nm data, which are less susceptible to solar

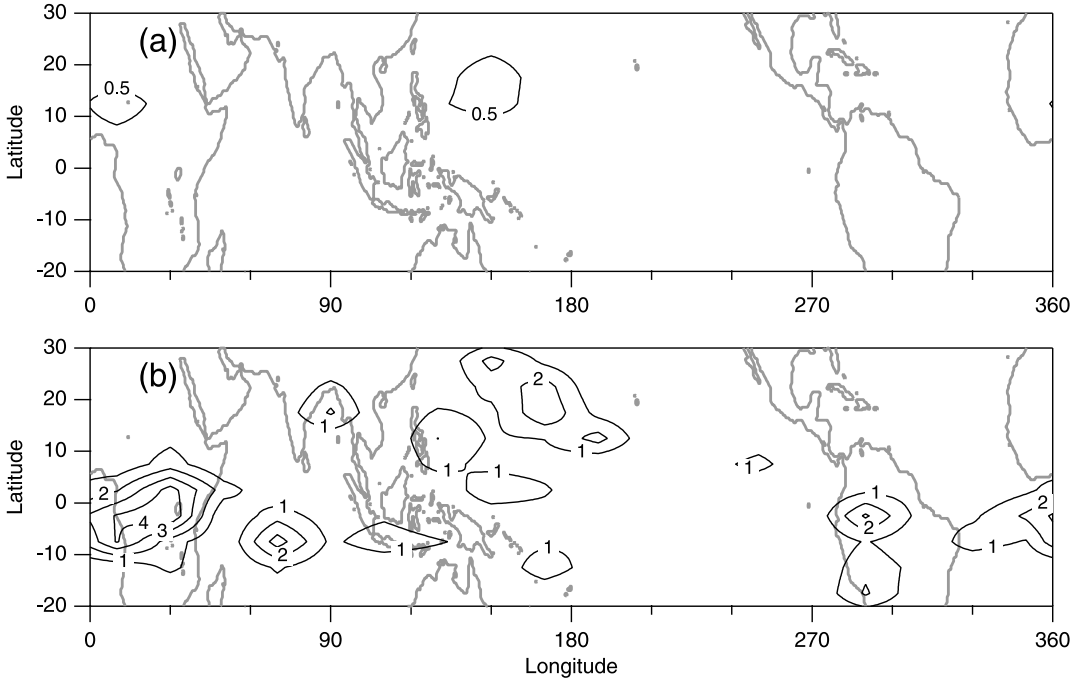

Figure 4. Fraction of GLAS observations (in percent) containing a TNTC at 400-K potential temperature, (a) morning data and (b) evening data. The contour interval is 0.5% for the morning plot and 1% for the evening plot.

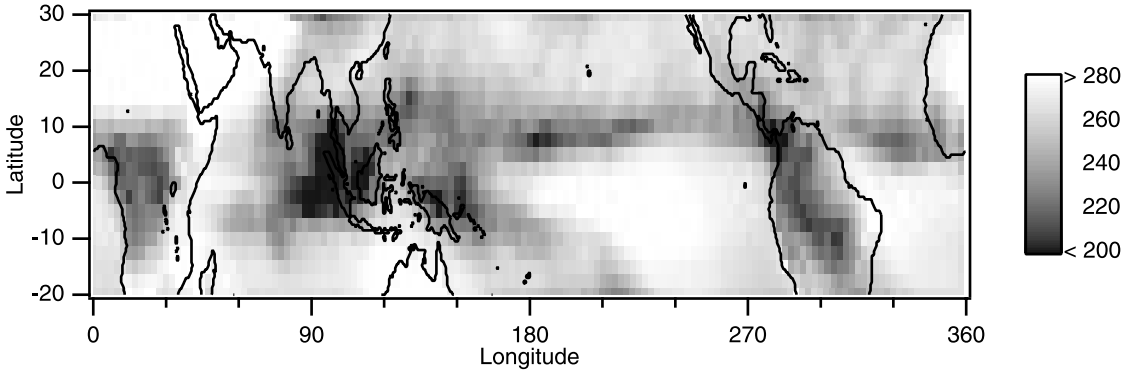

Figure 5. Outgoing longwave radiation (OLR) in W m^{-2} averaged over the Laser-2a period (29 September to 17 November 2003).

interference, to get a more accurate estimate of the diurnal cycle of TNTC occurrence, but we have not pursued that in this paper.

[16] The distribution shown is generally similar to the SAGE II thin cirrus climatology of *Wang et al.* [1996]. In the September-October-November panel of *Wang et al.* [1996, Plate 4], there are three maxima in the thin cirrus field: over Africa, South America, and the tropical western Pacific; this agrees well with GLAS data, which also show maxima in these regions. However, the exact locations of the maxima show some differences with the GLAS data, the most prominent being that the western Pacific maximum is located well to the north of the equator in the GLAS data at 370 and 377.5 K, but centered on the equator at 15.5 and 17.5 km in the SAGE II data (note that the Wang et al. figure is small, so it is difficult to confidently determine the exact latitude of the maximum). One plausible explanation is the differing time periods: SAGE II data were averaged over September, October, and November of a 6-year period (1985–1990), while GLAS data were obtained during one 7-week period of 2003.

[17] A more puzzling difference is that SAGE II sees far higher occurrence frequencies than GLAS. For example, SAGE II sees thin cirrus occurring >40% of the time at 17.5 km in the western Pacific. The GLAS data, however, show TNTC at 377.5 K occurring in 12% (evening) and 4% (morning) of the observations in this region. Similar differences between SAGE and GLAS occur in other locations and at other altitudes. The most obvious explanation for these differences in occurrence frequency concerns the differing viewing geometries of the satellites: SAGE II measures the integrated horizontal optical depth of the clouds, while GLAS measures the optical depth in the vertical. For clouds that fill the SAGE II field-of-view, optical depths as low as 2×10^{-4} km^{-1} are measurable. Such clouds could easily go undetected by GLAS. Additionally, optically thick clouds that fill a small fraction of the SAGE II field-of-view could also be counted as thin cirrus, but would not be counted as TNTC by GLAS.

[18] The lower frequencies observed by GLAS appear to be consistent with those from other lidar data sets. The Lidar In-Space Technology Experiment (LITE) made measurements for 53 hours during a flight of the space shuttle in September 1994, with a nighttime optical depth detection limit of 0.001–0.004, similar to GLAS. *Winker and Trepte* [1998] reported "laminar" cirrus (cloud top height > 15 km, thickness < 1 km) in about 14% of their nighttime tropical observations. GLAS sees such clouds in 11% of its nighttime observations over the same latitude range (20°S–30°N). *McFarquhar et al.* [2000] reported tropopause cirrus (cloud bottom height > 15 km) in 29% of their airborne lidar observations taken in March 1993 in the equatorial western Pacific, and these clouds had a mean thickness of 0.47 km. GLAS see such clouds in 22% of the nighttime observations between 10°N–10°S and 135°E–155°E, with a mean thickness of 0.69 km. Ground-based observations at Nauru Island (0.5°S, 166.9°E) detected single-layer cirrus with base heights > 15 km in 14% of the observations with an average thickness of 0.44 km [*Comstock et al.*, 2002]. Nighttime GLAS data taken around this site (3°S–3°N, 164°E–169°E) find clouds in 9% of the observations, with an average thickness of 0.99 km. Given the differences in the sampling periods of these data sets, the agreement appears reasonable.

4. Analysis

[19] To put the horizontal distribution of TNTC into context, we plot in Figure 5 outgoing longwave radiation (OLR), averaged over the laser-2a period (on the basis of the NOAA Interpolated OLR data set [*Liebmann and Smith*, 1996]). Low values of OLR indicate regions of deep cumulus convection. The OLR data show relatively confined minima over equatorial Africa and South America, as well as a broad minimum over the western Pacific. Also evident are the intertropical convergence zone and the South Pacific convergence zone.

[20] At all altitudes in the TTL, there is a general correspondence between TNTC maxima and OLR minima (this is a point also made by *Clark* [2005]). The coincidence is especially tight over equatorial Africa and South America. In the western Pacific, there are generally high values of TNTC frequency and generally low values of OLR. However, the details of the western Pacific's TNTC maxima do not line up exactly with the minima in OLR; for example, the OLR minimum at 90° longitude and over the equator is not collocated with a maximum in TNTC frequency. We will discuss this extensively later in this section.

[21] Figure 6 shows the average temperature of the 360-, 370-, 377.5-, and 400-K potential-temperature surfaces during the laser-2a period. As with OLR, there is a clear relationship between the TNTC frequency and temperature,

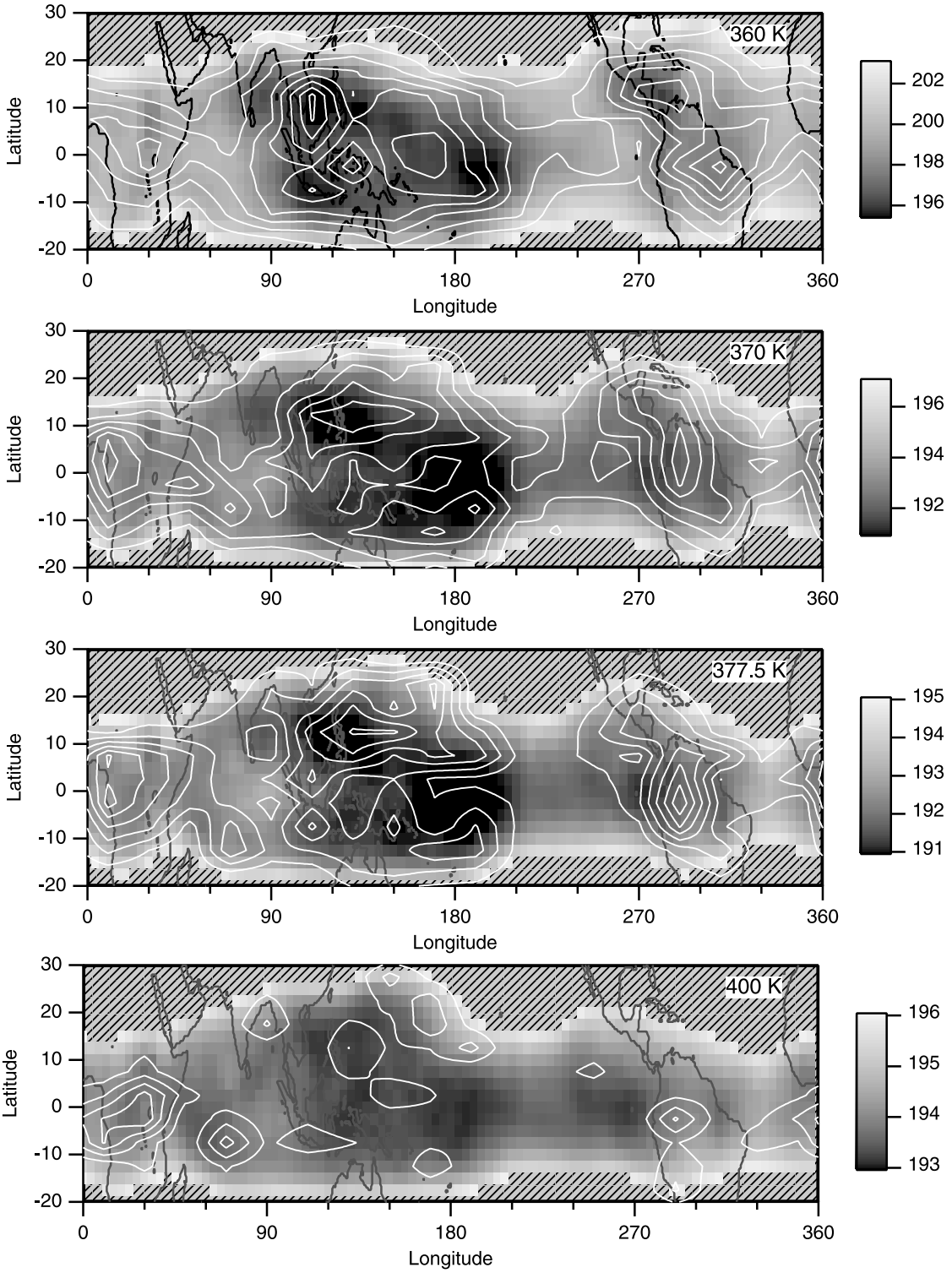

Figure 6. Average temperature (K) at 360-, 370-, 377.5-, and 400-K potential temperature based on UKMO meteorological fields. Also shown (white contours) is evening TNTC frequency from Figures 1–4.

with TNTC forming more frequently as the temperature decreases.

[22] To demonstrate the relationship between TNTC occurrence and TTL temperature more clearly, we have assigned to each GLAS measurement a temperature at 360, 370, 377.5 and 400 K by interpolating daily UKMO temperature fields to the GLAS measurement locations. In Figure 7, we show the fraction of GLAS measurements that contain a TNTC as a function of local temperature. Throughout the TTL, TNTC frequency increases as the local temperature decreases. This is consistent with our intuition, which suggests that clouds should form more frequently as the temperature decreases. The exception is at the coldest temperatures at 360 K, one sees that TNTC

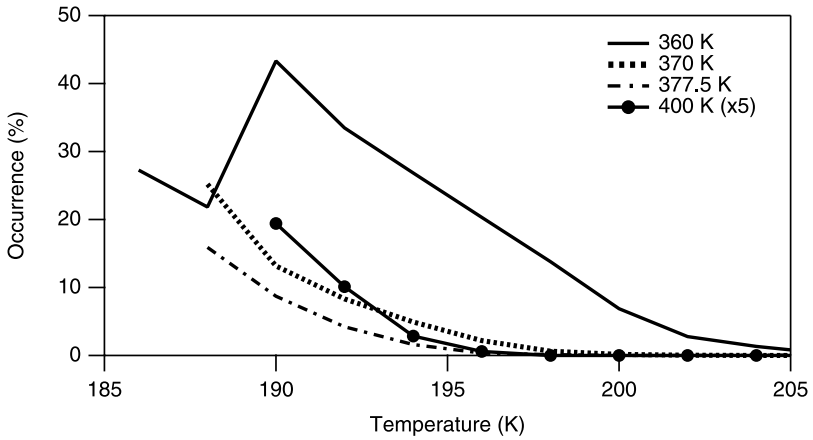

Figure 7. Fractional occurrence of TNTC (in percent) as a function of local temperature. The 400-K line has been multiplied by five for clarity. GLAS data were obtained in the evening and at latitudes between 20°S and 30°N.

frequency decreases as the temperature decreases. This behavior is somewhat puzzling, but without coincident measurements of water vapor, which are not available, we cannot unambiguously identify a reason for the behavior. It does, however, begin to suggest that, while temperature is important to TNTC formation, it is not the entire story.

[23] The decrease in TNTC frequency on the 360-K surface at the coldest temperatures is not the only puzzling aspect to the GLAS data. At 377.5-K potential temperature, for example, Figure 6 shows that TNTC frequencies greater than 12% occur over equatorial Africa and South America, but temperatures there are at least 1.5 K warmer than over the cold pool straddling the equator at 180° longitude, where TNTC frequencies are 2–6%. This stands in contrast to the trajectory-based microphysical model of Jensen and Pfister [*Jensen and Pfister*, 2004, 2005], which places the maximum thin cirrus occurrence at 380-K potential temperature where the temperatures are coldest, and predicts virtually no TNTC above continental convection over Africa and South America.

[24] We hypothesize that the presence of convection is playing a role in TNTC formation. To detangle the competing roles of temperature and convection on the formation of TNTC, we have also assigned to each GLAS measurement a value of OLR by interpolating the daily OLR fields to the location of each GLAS measurement. Next, we take all GLAS measurements in a 3-K temperature range (using the interpolated UKMO daily temperatures used in Figure 7) and plot the fraction of GLAS observations that observe a TNTC as a function of OLR. This is shown in Figure 8, broken into land and ocean data.

[25] Figure 8 shows that, at all levels in the TTL and at any fixed temperature, TNTC frequency increases as OLR decreases from ~300 W m^{-2} (i.e., clear skies) to ~200–250 W m^{-2} (relatively convective). The one exception is the oddly shaped 191-K line on the 360-K potential temperature surface over land, which we feel is likely a statistical anomaly. As OLR continues to decrease below ~200 W m^{-2}, the behavior is harder to characterize: at some altitudes and temperatures, TNTC frequency continues to increase; at others it decreases; at still others, it increases, then decreases.

[26] What can explain the increase in TNTC frequency as OLR decreases from 300 to 200 W m^{-2} at a fixed temperature? One possible explanation is that the UKMO temperatures have an OLR-dependent bias (i.e., the real temperature becomes progressively colder than the UKMO-reported temperature as OLR decreases). We tested this by doing the same analysis using the NCEP reanalysis [*Kalnay et al.*, 1996], and found the same result. This does not mean that a bias does not exist, but it does suggest that some aspect of the assimilation system that is common to these two systems would have to be responsible.

[27] One possible explanation that would be common to all assimilated temperature fields is the neglect of temperature fluctuations driven by waves that are not resolved by assimilation data systems, in particular, convectively generated gravity waves. Because these waves are generated by convective activity [e.g., *Pfister et al.*, 1993; *Alexander and Holton*, 1995; *Tsuda et al.*, 2000], we would expect their occurrence to correlate with OLR. If TNTC were forming during negative temperature fluctuations induced by gravity waves, then the trends in TNTC frequency in Figure 8 would make sense.

[28] The importance of temperature fluctuations has been discussed in the literature before: *Potter and Holton* [1995] speculated that temperature variations driven by convectively generated buoyancy waves may play a role in dehydrating the tropical lower stratosphere, while *Boehm and Verlinde* [2000] showed observational evidence that TNTC formed during wave-driven negative temperature fluctuations. *Comstock et al.* [2002] found a similar result for lower-level cirrus clouds.

[29] *Jensen and Pfister* [2004, section 2.2] discuss in detail the importance of unresolved variability for accurately simulating the cloud and water abundance of the TTL. To account for it, they added latitude-dependent but longitude-independent variability to the assimilated temperature fields driving their model. Their predicted cloud field shows no preference for TNTC to form over regions of intense continental convection, where GLAS finds abundant TNTC, likely a result of the longitude independence of their synthetic variability.

[30] *Gettelman et al.* [2002] added latitude- and longitude-independent synthetic variability to the assimilated temperature fields driving their model. Their model produ-

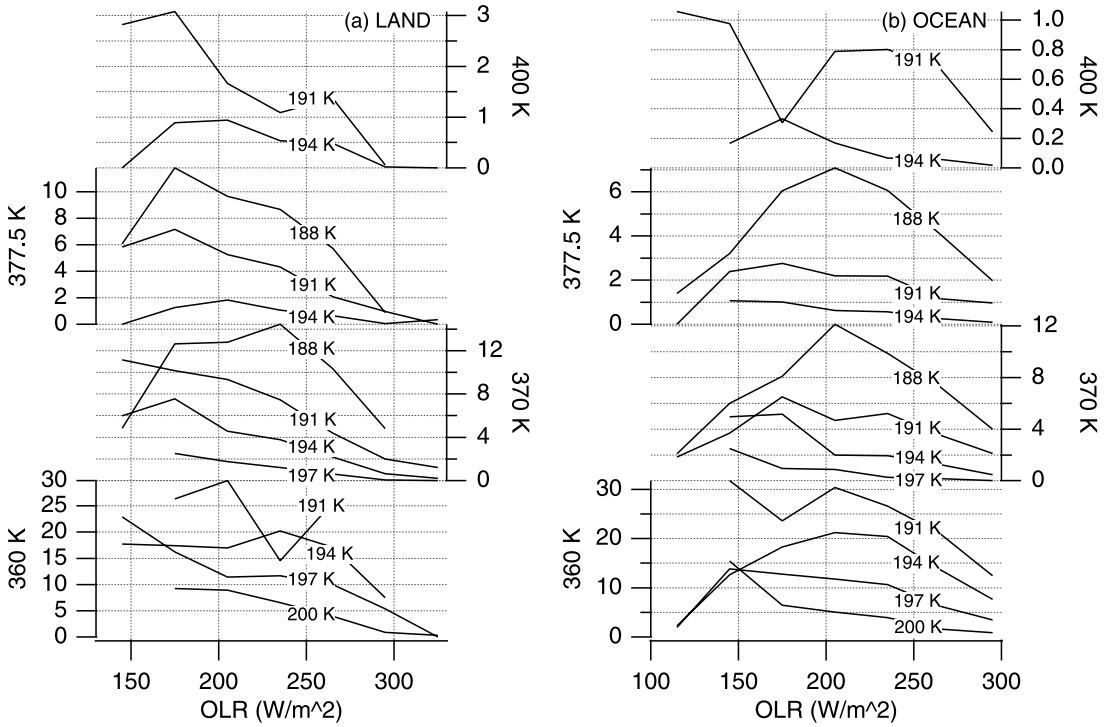

Figure 8. Fractional occurrence of TNTC (in percent) over (a) land and (b) ocean as a function of OLR at four potential temperature levels. Each line is constructed from GLAS observations within a 3-K temperature range and is marked with the minimum temperature of the bin; e.g., the 200-K line at 360-K potential temperature includes those GLAS measurements whose daily temperature at 360 K was between 200 and 203 K. Only temperature/OLR bins with at least 100 GLAS observations are included. GLAS data were obtained at latitudes between 20°S and 30°N.

ces simulations of continental maxima that are in reasonable qualitative agreement with satellite observations. We do not know why the model of Gettelman et al. more successfully predicts the continental maxima than the model of Jensen and Pfister despite less realistic synthetic variability.

[31] A second potential explanation for the observed OLR-dependence of the TNTC frequency is that TNTC are being directly injected into the TTL by convection. Analysis of tracer data [e.g., *Dessler*, 2002] has shown that convection does indeed transport significant mass to these altitudes, and analysis of satellite cloud data [e.g., *Massie et al.*, 2002; *Clark*, 2005] also supports this mechanism, so we must certainly consider this a possibility.

[32] We also note that the diverse behavior of the TNTC frequency as OLR decreases below 200 W m^{-2} (at some altitudes and temperatures, TNTC frequency increases to large values; at others, it goes to zero) suggests that other details besides temperature and OLR are important. For example, microphysical calculations [e.g., *Jensen et al.*, 1996, 2001] suggest that the formation of TNTC can be a function of parameters such as the rate of cooling or the size of the temperature perturbation, which are not necessarily well described by OLR. Neither are updraft velocity, overshoot height, and detrainment mass flux well constrained by OLR [e.g., *Sherwood et al.*, 2004].

[33] At the present time, we cannot determine the relative importance of in situ formation during wave-driven low-temperature excursions vs. direct injection of cloud material by convection on the TNTC distribution. It seems likely that both mechanisms are working, to some extent, but understanding the exact balance is crucially important. *Jensen and Pfister* [2004] argue that, if formed in situ, TNTC will almost always lead to dehydration of the TTL. TNTC directly injected by convection, on the other hand, might lead to hydration if the cloud particles evaporate in the TTL.

[34] In either case, our results suggest a revision of the cold-pool dehydration theory may be necessary. *Holton and Gettelman* [2001] used an idealized two-dimensional model to argue that dehydration occurs preferentially during horizontal transport through the "cold pool," the climatological cold region located over the equatorial western Pacific. Several investigators have followed up on this idea by using realistic trajectories driven by assimilated meteorological fields to more accurately examine the temperature history of the air entering the stratosphere [*Fueglistaler et al.*, 2004, 2005; *Bonazzola and Haynes*, 2004]. They find, in agreement with Holton and Gettelman, that the minimum temperature and saturation mixing ratio is experienced by parcels most often in the equatorial western Pacific cold pool [e.g., *Fueglistaler et al.*, 2005, Figure 5]). If the assumption is made that condensation and irreversible sedimentation occurs during these cold events, then reasonable values of stratospheric humidity can be simulated, including interannual variations.

[35] Our work here suggests the actual situation is more complicated. The GLAS data show that TNTC maxima form where assimilated temperatures are sufficiently low and coincident with convection. While dehydration may be

occurring in the cold pool, our results suggest that processes going on outside of the cold pool are also potentially important for understanding the abundance of water entering the stratosphere.

5. Conclusions

[36] In this paper, we have analyzed tropical cloud height data from the Geoscience Laser Altimeter System (GLAS), carried onboard the Ice, Cloud, and land Elevation Satellite (ICESat), obtained between 29 September and 17 November 2003 (the so-called "Laser 2a" period). These data provide a new view of the global distribution of thin, near-tropopause cirrus (TNTC).

[37] We have investigated the occurrence of TNTC at four potential temperatures: 360 K, around the base of the TTL; 370 K, about halfway between the base of the TTL and the tropopause; 377.5 K, the average height of the tropopause during this period; and 400 K, ~1 km above the tropopause.

[38] The GLAS data show that maxima in TNTC tend to occur over regions of intense convective activity: equatorial Africa and South America, both of which are the site for vigorous continental convection, and the western Pacific, which is a site of significant oceanic convection. Intriguingly, the GLAS see fewer clouds in the so-called "cold pool," a climatological temperature minimum located over the equatorial western Pacific where it has been suggested dehydration of air entering the stratosphere is occurring.

[39] Comparing assimilated temperatures with TNTC occurrence, we see that temperature clearly plays a role (Figure 7), but these temperatures are, by themselves, an incomplete predictor of the distribution of TNTC. At a fixed temperature, TNTC frequency generally increases as collocated outgoing longwave radiation (OLR) decreases (Figure 8), suggesting that convection plays a role in TNTC formation other than through its impact on synoptic-scale temperature of the TTL.

[40] We have not determined the physical mechanism that connects convection to TNTC occurrence. It might be due to temperature perturbations arising from convectively generated gravity waves, which are not resolved by assimilated meteorological systems. Or it might be due to direct injection of ice into the TTL by convection. This is a significant question. *Jensen and Pfister* [2004] argue that, if formed in situ, TNTC will almost always lead to dehydration of the TTL. TNTC directly injected by convection, on the other hand, might lead to hydration if the cloud particles evaporate in the TTL. Clearly, determining exactly what physical process is forming the TNTC is crucial for understanding the water budget of the TTL.

[41] Finally, we note that data analyzed in this paper come from a single period in late 2003, the Laser-2a period of the GLAS mission, and one for which no water vapor data were available. We must be cognizant that a longer data set, or one with more ancillary data, might reveal important new details and either confirm these results or show them to be a statistical abnormality. We look forward to analyzing other GLAS periods, as well as data from the upcoming Cloud-Aerosol Lidar and Infrared Pathfinder Satellite (CALIPSO) and Aura missions in order to gain a more thorough understanding of the issues.

[42] **Acknowledgments.** We would like to thank the ICESat/GLAS group for their hard work in creating this extraordinary data set. We would also like to thank Chris Shuman and Kris Barbieri for their help in interpreting the GLAS data. Useful comments from Ian Folkins, Eric Jensen, Steve Sherwood, and Bill Randel are gratefully acknowledged. This work was supported by NASA EOS/IDS and ACMAP grants, both to Texas A&M University. Interpolated OLR data are provided by the NOAA-CIRES ESRL/PSD Climate Diagnostics Branch, Boulder, Colorado, USA, from their Web site at http://www.cdc.noaa.gov/.

References

Alcala, C. M., and A. E. Dessler (2002), Observations of deep convection in the tropics using the TRMM precipitation radar, *J. Geophys. Res.*, *107*(D24), 4792, doi:10.1029/2002JD002457.

Alexander, M. J., and J. R. Holton (1995), Gravity waves momentum flux in the lower stratosphere over convection, *Geophys. Res. Lett.*, *22*, 2029–2032.

Atticks, M. G., and G. D. Robinson (1983), Some features of the structure of the tropical tropopause, *Q. J. R. Meteorol. Soc.*, *109*, 295–308.

Boehm, M. T., and J. Verlinde (2000), Stratospheric influence on upper tropospheric tropical cirrus, *Geophys. Res. Lett.*, *27*, 3209–3212.

Bonazzola, M., and P. H. Haynes (2004), A trajectory-based study of the tropical tropopause region, *J. Geophys. Res.*, *109*, D20112, doi:10.1029/2003JD004356.

Clark, H. L. (2005), Longitudinal variability of water vapor and cirrus in the tropical tropopause layer, *J. Geophys. Res.*, *110*, D07107, doi:10.1029/2004JD004943.

Comstock, J. M., T. P. Ackerman, and G. G. Mace (2002), Ground based lidar and radar remote sensing of tropical cirrus clouds at Nauru Island: Cloud statistics and radiative impacts, *J. Geophys. Res.*, *107*(D23), 4714, doi:10.1029/2002JD002203.

Dessler, A. E. (2002), The effect of deep, tropical convection on the tropical tropopause layer, *J. Geophys. Res.*, *107*(D3), 4033, doi:10.1029/2001JD000511.

Dessler, A. E., and P. Yang (2003), The distribution of tropical thin cirrus clouds inferred from Terra MODIS data, *J. Clim.*, *16*, 1241–1248.

Folkins, I., M. Loewenstein, J. Podolske, S. J. Oltmans, and M. Proffitt (1999), A 14 km mixing barrier in the tropics: Evidence from ozonesondes and aircraft measurements, *J. Geophys. Res.*, *104*, 22,095–22,102.

Fueglistaler, S., H. Wernli, and T. Peter (2004), Tropical troposphere-to-stratosphere transport inferred from trajectory calculations, *J. Geophys. Res.*, *109*, D03108, doi:10.1029/2003JD004069.

Fueglistaler, S., M. Bonazzola, P. H. Haynes, and T. Peter (2005), Stratospheric water vapor predicted from the Lagrangian temperature history of air entering the stratosphere in the tropics, *J. Geophys. Res.*, *110*, D08107, doi:10.1029/2004JD005516.

Gettelman, A., W. J. Randel, F. Wu, and S. T. Massie (2002), Transport of water vapor in the tropical tropopause layer, *Geophys. Res. Lett.*, *29*(1), 1009, doi:10.1029/2001GL013818.

Gettelman, A., P. M. D. Forster, M. Fujiwara, Q. Fu, H. Vomel, L. K. Gohar, C. Johanson, and M. Ammerman (2004), Radiation balance of the tropical tropopause layer, *J. Geophys. Res.*, *109*, D07103, doi:10.1029/2003JD004190.

Hajj, G. A., et al. (2004), CHAMP and SAC-C atmospheric occultation results and intercomparisons, *J. Geophys. Res.*, *109*, D06109, doi:10.1029/2003JD003909.

Hart, W. D., J. D. Spinhirne, S. P. Palm, and D. L. Hlavka (2005), Height distribution between cloud and aerosol layers in the Indian Ocean region from the GLAS spaceborne lidar, *Geophys. Res. Lett.*, *32*, L22S06, doi:10.1029/2005GL023671.

Hartmann, D. L., J. R. Holton, and Q. Fu (2001), The heat balance of the tropical tropopause, cirrus, and stratospheric dehydration, *Geophys. Res. Lett.*, *28*, 1969–1972.

Highwood, E. J., and B. J. Hoskins (1998), The tropical tropopause, *Q. J. R. Meteorol. Soc.*, *124*, 1579–1604.

Hlavka, D. L., S. P. Palm, W. D. Hart, J. D. Spinhirne, M. J. McGill, and E. J. Welton (2005), Aerosol and cloud optical depth from GLAS: Results and verifications for an October 2003 California fire smoke case, *Geophys. Res. Lett.*, *32*, L22S07, doi:10.1029/2005GL023413.

Holton, J. R., and A. Gettelman (2001), Horizontal transport and the dehydration of the stratosphere, *Geophys. Res. Lett.*, *28*, 2799–2802.

Jensen, E. J., and L. Pfister (2004), Transport and freeze-drying in the tropical tropopause layer, *J. Geophys. Res.*, *109*, D02207, doi:10.1029/2003JD004022.

Jensen, E., and L. Pfister (2005), Implications of persistent ice supersaturation in cold cirrus for stratospheric water vapor, *Geophys. Res. Lett.*, *32*, L01808, doi:10.1029/2004GL021125.

Jensen, E. J., O. B. Toon, H. B. Selkirk, J. D. Spinhirne, and M. R. Schoeberl (1996), On the formation and persistence of subvisible cirrus

clouds near the tropical tropopause, *J. Geophys. Res.*, *101*, 21,361–21,375.
Jensen, E. J., L. Pfister, A. S. Ackerman, A. Tabazadeh, and O. B. Toon (2001), A conceptual model of the dehydration of air due to freeze-drying by optically thin, laminar cirrus rising slowly across the tropical tropopause, *J. Geophys. Res.*, *106*, 17,237–17,252.
Kalnay, E., et al. (1996), The NCEP/NCAR 40-year reanalysis project, *Bull. Am. Meteorol. Soc.*, *77*, 437–471.
Liebmann, B., and C. A. Smith (1996), Description of a complete (interpolated) outgoing longwave radiation data set, *Bull. Am. Meteorol. Soc.*, *77*, 1275–1277.
Luo, B. P., et al. (2003), Dehydration potential of ultrathin clouds at the tropical tropopause, *Geophys. Res. Lett.*, *30*(11), 1557, doi:10.1029/2002GL016737.
Massie, S., A. Gettelman, W. Randel, and D. Baumgardner (2002), The distribution of tropical cirrus in relation to convection, *J. Geophys. Res.*, *107*(D21), 4591, doi:10.1029/2001JD001293.
McFarquhar, G. M., A. J. Heymsfield, J. Spinhirne, and B. Hart (2000), Thin and subvisual tropopause tropical cirrus: Observations and radiative impacts, *J. Atmos. Sci.*, *57*, 1841–1853.
Mergenthaler, J. L., A. E. Roche, J. B. Kumer, and G. A. Ely (1999), Cryogenic Limb Array Etalon Spectrometer observations of tropical cirrus, *J. Geophys. Res.*, *104*, 22,183–22,194.
Nee, J. B., C. N. Len, W. N. Chen, and C. I. Lin (1998), Lidar observation of the cirrus cloud in the tropopause at Chung-Li (25 degrees N, 121 degrees E), *J. Atmos. Sci.*, *55*, 2249–2257.
Palm, S., W. Hart, D. Hlavka, E. J. Welton, A. Mahesh, and J. Spinhirne (2002), Geosciences Laser Altimeter System (GLAS) Atmospheric data products, Algorithm theoretical basis document, version 4.2, 137 pp., NASA Goddard Space Flight Cent., Greenbelt, Md.
Peter, T., et al. (2003), Ultrathin tropical tropopause clouds (UTTCs): I. Cloud morphology and occurrence, *Atmos. Chem. Phys.*, *3*, 1083–1091.
Pfister, L., K. R. Chan, T. P. Bui, S. Bowen, M. Legg, B. Gary, K. Kelly, M. Proffitt, and W. Starr (1993), Gravity waves generated by a tropical cyclone during the STEP tropical field program, *J. Geophys. Res.*, *98*, 8611–8638.
Potter, B. E., and J. R. Holton (1995), The role of monsoon convection in the dehydration of the lower tropical stratosphere, *J. Atmos. Sci.*, *52*, 1034–1050.
Randel, W. J., F. Wu, and D. J. Gaffen (2000), Interannual variability of the tropical tropopause derived from radiosonde data and NCEP reanalysis, *J. Geophys. Res.*, *105*, 15,509–15,523.
Randel, W. J., F. Wu, and W. R. Rios (2003), Thermal variability of the tropical tropopause region derived from GPS/MET observations, *J. Geophys. Res.*, *108*(D1), 4024, doi:10.1029/2002JD002595.
Rocken, C., et al. (1997), Analysis and validation of GPS/MET data in the neutral atmosphere, *J. Geophys. Res.*, *102*, 29,849–29,866.
Sassen, K., and B. S. Cho (1992), Subvisual thin cirrus lidar dataset for satellite verification and climatological research, *J. Appl. Meteorol.*, *31*, 1275–1285.
Sherwood, S. C., and A. E. Dessler (2000), On the control of stratospheric humidity, *Geophys. Res. Lett.*, *27*, 2513–2516.
Sherwood, S. C., and A. E. Dessler (2001), A model for transport across the tropical tropopause, *J. Atmos. Sci.*, *58*, 765–779.
Sherwood, S. C., J.-H. Chae, P. Minnis, and M. McGill (2004), Underestimation of deep convective cloud tops by thermal imagery, *Geophys. Res. Lett.*, *31*, L11102, doi:10.1029/2004GL019699.
Spinhirne, J. D., S. P. Palm, W. D. Hart, D. L. Hlavka, and E. J. Welton (2005), Cloud and aerosol measurements from GLAS: Overview and initial results, *Geophys. Res. Lett.*, *32*, L22S03, doi:10.1029/2005GL023507.
Swinbank, R., and A. O'Neill (1994), A stratosphere-troposphere data assimilation system, *Mon. Weather Rev.*, *122*, 686–702.
Tsuda, T., M. Nishida, C. Rocken, and R. H. Ware (2000), A global morphology of gravity wave activity in the stratosphere revealed by the GPS occultation data (GPS/MET), *J. Geophys. Res.*, *105*, 7257–7273.
Wang, P. H., P. Minnis, M. P. McCormick, G. S. Kent, and K. M. Skeens (1996), A 6-year climatology of cloud occurrence frequency from stratospheric aerosol and gas experiment II observations (1985–1990), *J. Geophys. Res.*, *101*, 29,407–29,429.
Winker, D. M., and C. R. Trepte (1998), Laminar cirrus observed near the tropical tropopause by LITE, *Geophys. Res. Lett.*, *25*, 3351–3354.
Zwally, H. J., et al. (2002), ICESat's laser measurements of polar ice, atmosphere, ocean, and land, *Geodynamics*, *34*, 405–445.

A. E. Dessler, Department of Atmospheric Sciences, Texas A&M University, TAMU 3150, College Station, TX 77843, USA. (adessler@tamu.edu)
W. D. Hart and S. P. Palm, Science Systems and Applications Inc., Lanham, MD 20706, USA.
J. D. Spinhirne, NASA Goddard Space Flight Center, Greenbelt, MD 20771, USA.